Chemically Resolved Imaging of Biological Cells and Thin Films by Infrared Scanning Near-Field Optical Microscopy

Antonio Cricenti,* Renato Generosi,* Marco Luce,* Paolo Perfetti,* Giorgio Margaritondo,† David Talley,‡ Jas S. Sanghera,‡ Ishwar D. Aggarwal,‡ Norman H. Tolk,§ Agostina Congiu-Castellano,¶ Mark A. Rizzo,|| and David W. Piston||

*Istituto di Stuttura della Materia, Rome, Italy; †Institut de Physique Appliquée, Ecole Polytecnique Fédérale, Lausanne, Switzerland; ‡Optical Sciences Division, U.S. Naval Research Laboratory, Washington, District of Columbia; §Department of Physics and Astronomy, Vanderbilt University, Nashville, Tennessee; ¶Department of Physics, Università di Roma "La Sapienza," Rome, Italy; and ||Department of Molecular Physiology and Biophysics, Vanderbilt University, Nashville, Tennessee

ABSTRACT The infrared (IR) absorption of a biological system can potentially report on fundamentally important microchemical properties. For example, molecular IR profiles are known to change during increases in metabolic flux, protein phosphorylation, or proteolytic cleavage. However, practical implementation of intracellular IR imaging has been problematic because the diffraction limit of conventional infrared microscopy results in low spatial resolution. We have overcome this limitation by using an IR spectroscopic version of scanning near-field optical microscopy (SNOM), in conjunction with a tunable free-electron laser source. The results presented here clearly reveal different chemical constituents in thin films and biological cells. The space distribution of specific chemical species was obtained by taking SNOM images at IR wavelengths (λ) corresponding to stretch absorption bands of common biochemical bonds, such as the amide bond. In our SNOM implementation, this chemical sensitivity is combined with a lateral resolution of 0.1 μm ($\approx\lambda/70$), well below the diffraction limit of standard infrared microscopy. The potential applications of this approach touch virtually every aspect of the life sciences and medical research, as well as problems in materials science, chemistry, physics, and environmental research.

INTRODUCTION

Infrared (IR) spectroscopy is a well-established tool in materials and life-science research. IR microscopy has also found important applications in solid-state science and in biology (Carr et al., 1998 and references therein). These applications have been further developed using the superior brightness of synchrotron sources. Due to the long wavelength of IR light, however, the lateral resolution of conventional IR microscopy is limited to a few microns, which precludes the use of IR microscopy for subcellular imaging applications in modern biology. Still, spectrally-resolved IR imaging of single cells has recently been demonstrated (Lasch et al., 2002), and holds considerable promise for biological research. The diffraction limit can be bypassed using a near-field optical approach, such as scanning near-field microscopy (SNOM) (Betzig and Trautman, 1992; Betzig et al., 1992; Heinzelmann and Pohl, 1994, Pohl and Courjon, 1992; Almeida et al., 1996; Cricenti et al., 1998a). One particularly promising approach is ''aperture-less'' SNOM (Zenhausern et al., 1995, Knoll and Keilmann, 1999), that has been used to image different samples with nanometric resolution. This approach should be useful for IR imaging in biological applications, but such applications have not yet been described using this configuration. However, the apertureless approach will not be useful for samples under water, which is our ultimate goal for biological systems.

In this work, we use a reflection SNOM system, where the entire sample is illuminated by the IR light, and the reflected signal is collected with a narrow fiber tip aperture ($<\lambda$) placed at a distance smaller than λ from the sample surface. The use of SNOM allows us to greatly surpass the diffraction-limited resolution, and easily visualize subcellular structures. The full potential of IR-SNOM, however, is not exploited without using a *spectroscopic* approach, i.e., taking images at different wavelengths to detect specific vibrational modes characteristic of chemical constituents (Piednoir et al., 1996). The power of such a spectroscopic approach in IR-SNOM has been demonstrated in semiconductors, polymers, and organic chemical systems (Cricenti et al., 1998a,b; Piednoir et al., 1996; Palanker et al., 1998; Hong et al., 1998). Here, we describe our results using this approach to image biological systems, including live cells.

METHODS

SNOM imaging

In our experimental setup, IR photons from the unfocused free-electron laser (FEL) beam are directed by a mirror onto the sample surface at an $\sim$75° angle to the surface normal. Reflected photons are detected through a narrow-point optical fiber tip mounted on a SNOM module, which also measures shear-force (topographic) images (Cricenti et al., 1998c). During a scan, reflected IR light is picked up through the fiber and is detected by an MCT photoconductive detector (Hamamatsu P2750). Topographical and optical images were taken simultaneously, with the FEL illuminating the specimen over a broad area ($\sim$1-mm spot diameter) and the SNOM probe collecting the reflected light. The shear-force signal is independently used to keep the

Submitted March 24, 2003, and accepted for publication July 18, 2003.

Address reprint requests to David W. Piston, 702 Light Hall, Vanderbilt University, Nashville, TN 37232-0615. Tel.: 615-322-7030; Fax: 615-322-7236; E-mail: dave.piston@vanderbilt.edu.

0006-3495/03/10/2705/06 $2.00

tip-surface interaction force constant while taking SNOM images. In this mode, the data are collected at a preset value of the shear force between sample and tip. This force should be kept constant when scanning the sample to have a constant shear force image (topography). At the same time, the SNOM acquire the optical data at a distance, presumably kept constant during the scan. In a synchronous scan, data points are taken at a fixed time (decided at the beginning of the image), and the quality of the image depends on the speed of the electromechanical system (feedback) to follow the corrugation of the sample. If the sample is flat, the variation of signal is small and the feedback can easily follow the local corrugation. However, if the sample is highly corrugated, then the feedback system will take a longer time to follow the real corrugation of the sample. In general, if there is a mixed roughness in the sample, then the feedback will work differently at the different positions of the sample. In a synchronous data acquisition the data points are taken independently of the conditions of the feedback, i.e., the system is not working correctly at constant shear force. In this case, the different distances also affect the local optical properties, and the optical image will exhibit the same structures seen in the topography. An advantage of the asynchronous data acquisition used in our work is the fact that the *error signal* (i.e., the difference between the feedback signal and the reference voltage) is negligible. In fact, a data point is stored only when the feedback signal equals the reference signal, i.e., the applied force is really constant for all data points.

Fiber tip probes

Infrared SNOM probes were obtained from single-mode, one-meter-long, arsenic selenide fibers having a 50-μm-clad diameter and a 100-μm-core diameter. One end of the fiber is interfaced to a InSb detector while the remaining end of the fiber was chemically etched using a protective layer etching system (Talley et al., 2000). The etched tips were then coated with gold with an approximate coating thickness of 100–125 nm.

Cell culture

INS-1 cells were seeded on glass cover slides. After 24 h the medium was removed and the cells were fixed in paraformaldehyde and washed twice with phosphate-buffered saline (PBS) and twice with distilled water. COS-7 cells were grown and plated on coverslips in Dulbecco's Modified Eagles Medium. Once cells were ~50% confluent, the media was replaced with a small amount of PBS, which was partially dried, and the cells were imaged immediately.

RESULTS

One major component needed for spectroscopic IR-SNOM is the appropriate IR light source that is both tunable over a broad band to cover the relevant vibrational modes and intense enough to compensate for the limited light transmission of the narrow fiber tip. To meet these requirements, previous reports have used a free electron laser, or FEL (Palanker et al., 1998; Hong et al., 1998; Cricenti et al., 1998b), or an optical parametric amplifier (Michaels et al., 2000). Each method has its strengths and weaknesses (e.g., the FEL is more expensive to build, but very reliable). For the experiments described here, we used an FEL source. Although any tunable IR laser should perform in an equivalent manner, the Vanderbilt Mark III FEL conveniently provides a broad tuning range of 1–10 μm, which is ideal for IR-SNOM applications in biology (Tuncel et al., 1993; Coluzza et al., 1992).

Our experiments were performed with a multitechnique SNOM module (Cricenti et al., 1998c). This instrument can deliver shear-force (topographic) images as well as reflectivity SNOM images, by using an asynchronous scanning approach that eliminates topographic artifacts in the SNOM images. This direct comparison of topographic and spectroscopic SNOM images is essential to prove the resolution of the SNOM images. The fabrication of extremely high quality infrared fiber tips (Talley et al., 2000) was a crucial step in the practical implementation of our technique. Details about the experimental design and fiber tips are given in the Methods section. By combining the tunable IR source with the high quality IR fiber tips, we were able to investigate the IR signatures from mammalian cells with submicron resolution.

Using this IR-SNOM instrument that was optimized for cell biological applications, we first performed a series of experiments on thin films of biofilm growth media. These thin films provide excellent two-dimensional chemical contrast, and allow for a quantitative determination of the lateral resolution of our IR-SNOM system (Cricenti et al., 2002). The films were prepared by submerging a thick silicon substrate in a postgate growth medium solution for several minutes at room temperature, then dipping the substrate in deionized water, and allowing it to dry for one day.

The film-covered areas of the substrate were analyzed first with an optical microscope and then with the SNOM. The growth medium is composed of several constituents (de Beer et al., 1994), primarily sulfur and nitrogen-oxide compounds, whose vibrational stretch mode absorption occurs at ~7 μm (van der Maas, 1972). To test this point explicitly, we performed Fourier transform infrared spectroscopy (FTIR) on this sample, which showed a deep minimum in the transmission at ~7 μm (data not shown). SNOM images were taken at $\lambda = 6.95$ and 6.6 μm, i.e., inside and outside the absorption region measured by FTIR.

Fig. 1 shows 20×20 μm^2 reflection-SNOM images together with the corresponding shear-force topography images. In the SNOM images, darker areas correspond to stronger absorption. The contrast between the featureless off-absorption image and the rich microstructures observed in the on-absorption image is quite striking. The off-absorption image also shows that the optical and electronic noise is 0.003–0.004 mV, i.e., ~15% of the signal. The comparison between the 6.95-μm SNOM image (Fig. 1 *c*) with the shear-force image (Fig. 1 *d*) shows that its microstructures are indeed related to the growth medium constituents and not just artifacts. Similar topographic images are observed for both wavelengths (compare Fig. 1, *b* and *d*) and reveal biological growth medium grains with width and height of a few microns. If the 6.95-μm SNOM image was an artifact of the topography, we would expect to see the same artifact in the 6.6-μm SNOM image. The lateral resolution of the topographic and spectroscopic-SNOM images was deter-

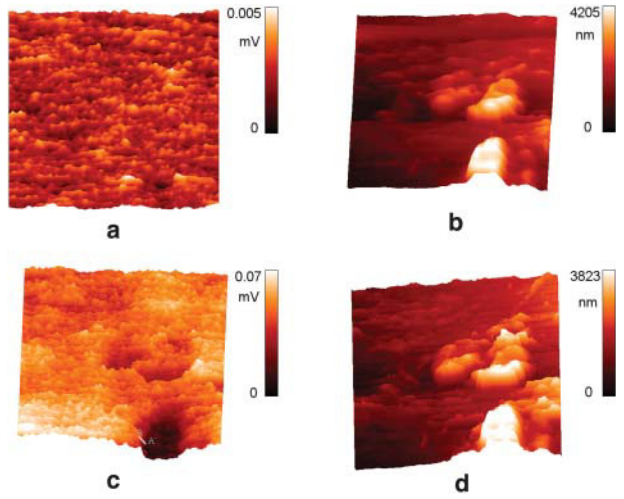

FIGURE 1 (*Left*) $20 \times 20\ \mu m^2$ SNOM reflection images obtained with (*c*) $\lambda = 6.95\ \mu m$ photons, corresponding to the vibrational stretch mode absorption bands of sulfur and nitrogen-oxide compounds, and with a wavelength outside the absorption region, (*a*) $\lambda = 6.6\ \mu m$. Darker areas correspond to stronger absorption. (*Right*) Corresponding shear-force (topographic) images; brighter areas correspond to higher topography values. All the images shown here and in the following figures are unfiltered and are raw results, except for subtraction of a constant background.

mined from line scans to be 50–80 nm for the topographic images (Fig. 2 *b*, which demonstrates the high quality of the fiber tips) and 100 nm for the corresponding spectroscopic SNOM image (Fig. 2 *a*). This value for optical resolution is well below the diffraction limit ($\lambda/2$), and corresponds to $\sim\lambda/70$ at 6.95 μm.

A second series of experiments was conducted on tissue culture cells. We first imaged cells from a rat pancreatic β-cell line (INS-1); see Fig. 3. Since these cells were fixed, we could rinse them with pure water and dry them before SNOM imaging. Once again, the shear-force topography images were independent of the wavelength (Fig. 3, *a*, *c*, and *e*) and the SNOM images dramatically different for different wavelengths. The images for $\lambda = 6.1\ \mu m$ (amide I, *C=O* stretch band; Fig. 3 *b*) and $\lambda = 6.95\ \mu m$ (sulfide stretch band; Fig. 3 *f*) show absorption within the cell, as opposed to the $\lambda = 6.45$-μm image (Fig. 3 *d*), which shows much less contrast. Although we would expect absorption in the cell at both the amide I band (6.1 μm) and the amide II band (6.45 μm), the contrast mechanism in the images is not solely governed by the cellular properties, but also by the properties of the background. This can be seen in Fig. 3, *b* and *f*, where the reflected signal outside the cell is larger than it is in Fig. 3 *d*. Thus, the contrast at 6.1 μm and 6.95 μm is larger than it is for 6.45 μm.

Finally, we performed experiments at several different wavelengths on COS-7 cells that had not been fixed: the cells were dried in buffer and imaged immediately with just a thin coating of aqueous buffer. As shown in Fig. 4 *a*, cells could be detected by shear-force topography, but crystals of the PBS were also clearly observed. The topographic images

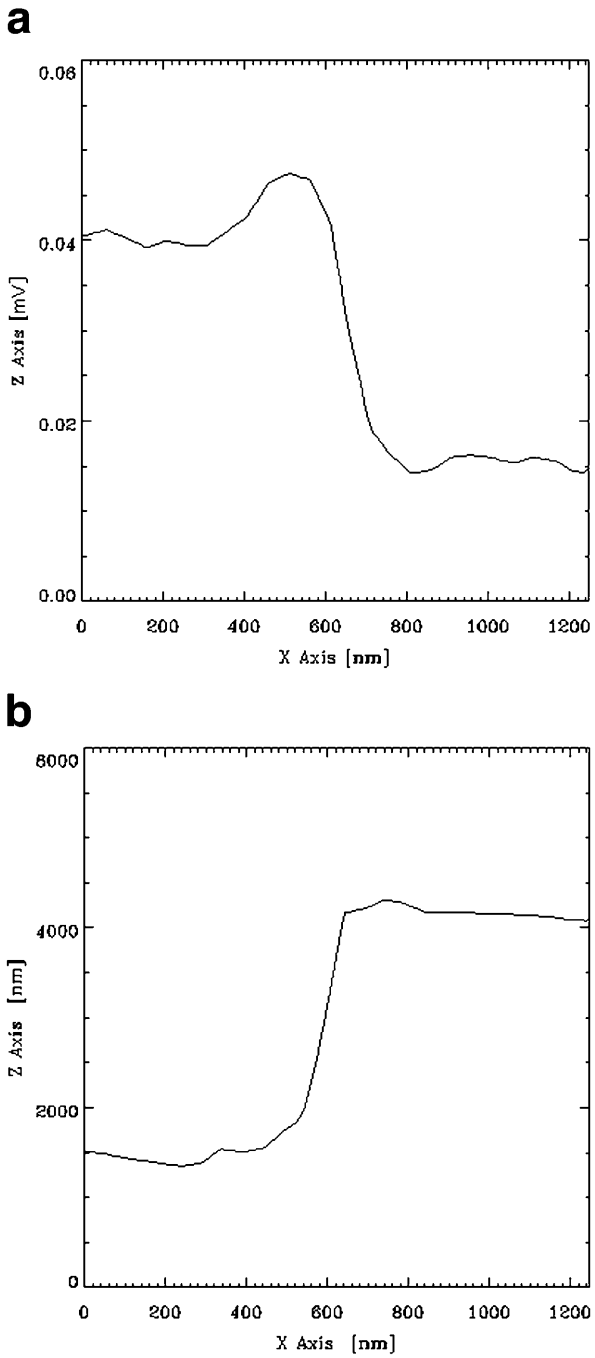

FIGURE 2 (*a*) Intensity profile taken along the *A*-*A*′ line on the SNOM reflectivity image with $\lambda = 6.95\ \mu m$ (see Fig. 1 *c*) and (*b*) the same profile taken from the topography image (see Fig. 1 *d*).

were once again λ-independent. The SNOM images, however, were seen to be strongly dependent on the wavelength. In particular, the 8.05-μm image (Fig. 4 *b*) corresponding to the phosphate stretch band shows the PBS crystal as an extremely dark object, and also reveals absorption in the region of the cell nucleus. Differences in absorption are visible between the cell and the crystal: for example, only the crystal reflects at 7.6 μm (Fig. 4 *c*).

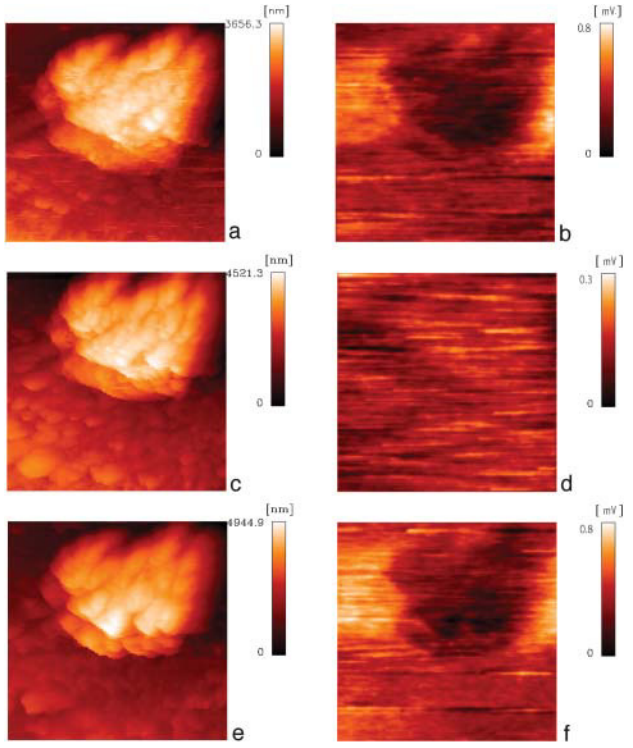

FIGURE 3 $20 \times 20\ \mu m^2$ SNOM reflection images of an INS-1 cell in water under illumination with (*b*) $\lambda = 6.1\ \mu m$, (*d*) $\lambda = 6.45\ \mu m$, and (*f*) $\lambda = 6.95\ \mu m$. Also shown are the corresponding shear-force (topographic) images (*a*, *c*, and *e*).

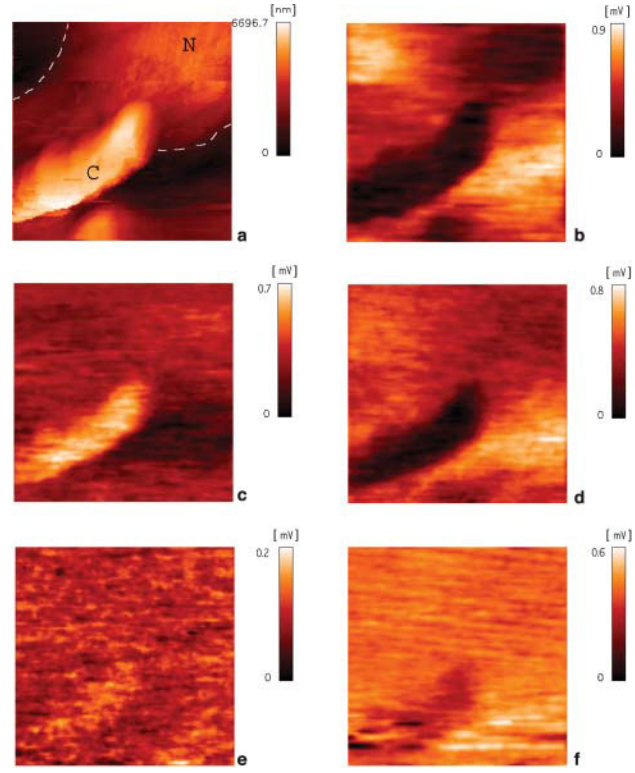

FIGURE 4 (*a*) $20 \times 20\ \mu m^2$ shear-force (topographic) image of a COS-7 cell in PBS. The cell body and nucleus (*upper right*) are seen and a crystal of PBS (*left side*) can also be seen on the cell. SNOM reflection images of the same field were obtained under illumination with (*b*) $\lambda = 8.05\ \mu m$, (*c*) $\lambda = 7.6\ \mu m$, (*d*) $\lambda = 6.95\ \mu m$, (*e*) $\lambda = 6.45\ \mu m$, and (*f*) $\lambda = 6.1\ \mu m$.

Absorption is seen throughout the cell at 6.95 μm (Fig. 4 *d*), whereas the nucleus has the strongest absorption at 8.05 μm (Fig. 4 *b*).

DISCUSSION

Our results constitute the first practical implementation of IR near-field microscopy for cell biological applications. The key elements leading to success were the use of a highly reliable homemade SNOM module (mechanics, electronics, and asynchronous data acquisition), a tunable IR source (in this case a near-infrared FEL) and the exceptional quality of the optical fibers. This system yields a spatial resolution in shear-force images of ~50 nm, and an optical resolution of ~100 nm, which is $\lambda/70$ in the IR. This optical resolution is even smaller than that obtained from conventional optical microscopy in the visible, with the added chemical resolution arising from the tunable, monochromatic source.

There are three separate pieces of evidence that support this determination of optical resolution, and show that it is not an artifact of the sample topology. First, the resolution is different between the topology image and the optical image (see Fig. 2). This suggests that the two resolutions are not directly related. Secondly, if we relax the zero error signal criteria for our asynchronous scanning, we do begin to observe a topographical artifact in the optical channel. This further indicates that the asynchronous scan eliminates topographical artifacts in the optical image. Finally, we see no topographical artifacts in optical images taken with IR wavelengths where there is no optical absorption. Topographical artifacts should be visible at all wavelengths and be independent of the optical absorption. All images at all wavelengths from many different samples confirm the conclusion that the optical resolution seen in our experiments is not due to a topographical artifact.

Another way to eliminate topological artifacts is to image using the constant height mode. However, a disadvantage to using the constant height mode is that it is performed by acquiring the images after retracting the fiber 100–200 nm from the sample. This greatly reduces the strength of the near-field conditions, and in practice no more small structures (smaller than the wavelength used) are observed in the optical image (see Fig. 7 of Williamson et al., 1998). By retracting the fiber, the sensitivity to the near-field is reduced. Thus, our constant shear force mode with asynchronous data acquisition offers the best optical resolution while reducing the topographic artifacts in the optical image.

Perhaps the most important advance that allowed the imaging described here is the use of a shear-force scanning

protocol, which allows SNOM imaging with asynchronous scanning (Cricenti et al., 1998c). This approach attempts to keep the tip-to-surface distance constant throughout the experiment by using the shear-force signal. Each SNOM pixel is acquired only after the correct distance has been achieved. After a large topographical step, the equilibration time for the shear-force signal is longer, but the asynchronous scanning waits to acquire the SNOM signal until the shear-force signal is equilibrated. This data acquisition protocol causes the scanning speed to be dependent on the degree of surface roughness: the rougher the surface, the slower the scan. An advantage of this asynchronous data acquisition is the fact that the error signal is negligible. In the synchronous data acquisition system used by many other groups, the data points are acquired at preset time-points independent of the value of the error signal. The result is that the noise level in an image can be very high, particularly for modulation experiments (like tapping mode, noncontact atomic force microscopy, and shear-force SNOM). This is not the case of our system: in fact a data point is stored only when the applied force is really constant for all data points. In this fashion, our SNOM experiments are not subject to topographical artifacts, and the true optical resolution can be determined from the SNOM images. In the case of the biofilm, where sharp edges are expected, we achieved optical resolutions of 100 nm, which is $\lambda/70$ for the IR wavelengths used in our experiments.

Another key factor that made these results possible is the high quality of the IR-compatible fiber tips (Talley et al., 2000). First, the IR signal collected through the tips is sufficient throughout the IR region from 1 to 10 μm, and this allows us to probe many of the biologically important IR absorption bands. The quality of these tips can also be seen in the superb lateral topographical resolution of our data, which is >50 nm. This topographical resolution nicely complements the optical signal resolution as discussed above. Both the optical and topographical resolutions are comparable with those attained by conventional optical microscopy using visible wavelengths.

The images shown in Figs. 3 and 4 show the differences in complex contrast expected at different wavelengths, as well as some surprising results. Most striking is the near featureless images taken with 6.45 μm (Figs. 3 *d* and 4 *e*). This indicates that there is uniform absorption from all of the material deposited on the coverslip (i.e., cells, precipitated crystal, background). This is consistent with all of our images acquired with 6.45 μm, confirming that absorption from the amide II band is spread out throughout the sample. It is worth noting that the strongest absorption in Fig. 3 (pancreatic cells) is at 6.1 μm (amide I band), consistent with FTIR spectra of cultured cells, which shows the strongest absorbing region to be the amide I band (Diem et al., 1999 and references therein).

In the case of the COS-7 cells, the strongest absorption is at 8.05 μm, corresponding to the phosphate region associated with RNA and DNA. This result may be due to the localization of the DNA nuclei, which yields a strong local absorption seen in the SNOM image, but a relatively low absorption in the FTIR measurements. Such absorption has been seen in FTIR, for example, in cells during replication, possibly because of the spatial extension increase of the nucleus (Diem et al., 1999). By using SNOM, it is possible to reveal a more accurate estimation of the chemical composition due to the small field of view given by the high-resolution (small tip aperture). In this case, the dense-packed nucleus can be easily detected because of the relative increase in absorption compared to the background. Of course, in these experiments, a possible contribution from precipitated PBS solution onto the surface of the cell cannot be totally excluded. Future experiments using the high resolution SNOM approach will help elucidate these issues.

Finally, we were able to achieve chemical resolution by scanning through the IR wavelengths with a tunable, monochromatic source. In our experiments, we used the Mark III FEL operating in the Keck FEL Center at Vanderbilt University. For reflected light SNOM imaging applications, only a modest incident intensity is required, so the FEL beam must be attenuated by several orders of magnitude. Because only low intensities are needed for these experiments, they would also be possible using optical parametric oscillator systems, which have previously been used for similar SNOM experiments (Michaels et al., 2000).

We emphasize that no insurmountable obstacles exist that would disallow the use of this approach for live cellular systems. Similar measurements will be possible on samples submerged in water by using both illumination and detection through the same fiber tip. In this case, it is not possible to perform measurements using the more popular apertureless mode, which has been a large motivation for this current work. Future potential applications include, for example, a wide variety of biological, polymer, and semiconductor (Margaritondo et al., 1993) systems.

We thank the entire staff of the W. M. Keck Foundation Free Electron Laser Center at Vanderbilt University for their able assistance.

This work is supported by the Italian National Research Council, Ecole Polytechnique Fédérale de Lausanne, the Fonds National Suisse de la Recherche Scientifique, the National Institutes of Health, the United States Office of Naval Research, and the United States Air Force Office of Scientific Research.

REFERENCES

Almeida, J., T. dell'Orto, C. Coluzza, G. Margaritondo, O. Bergossi, M. Spajer, and D. Courjon. 1996. Novel spectromicroscopy: Pt-GaP studies by spatially resolved internal photoemission with near-field optics. *Appl. Phys. Lett.* 69:2361–2363.

Betzig, E., and J. K. Trautman. 1992. Near-field optics: microscopy, spectroscopy, and surface modification beyond the diffraction limit. *Science*. 257:189–195.

Betzig, E., P. L. Finn, and J. S. Wiener. 1992. Combined shear force and near-field scanning optical microscopy. *Appl. Phys. Lett.* 60:2484–2486.

Carr, G. L., P. Dumas, C. J. Hirschmugl, and G. P. Williams. 1998. Infrared synchrotron radiation programs at the National Synchrotron Light Source. *Il Nuovo Cimento*. 20:375–395.

Coluzza, C., E. Tuncel, J. L. Staehli, P. A. Baudat, G. Margaritondo, J. T. McKinley, R. G. Albridge, A. V. Barnes, A. Ueda, N. H. Tolk, D. Martin, F. Morier-Genoud, C. Dupuy, A. Rudra, and M. Ilegems. 1992. Interface measurements of heterojunction band lineups with the Vanderbilt free-electron laser. *Phys. Rev. B*. 46:12834–12836.

Cricenti, A., R. Generosi, P. Perfetti, J. M. Gilligan, N. H. Tolk, C. Coluzza, and G. Margaritondo. 1998a. Free-electron-laser near-field nanospectroscopy. *Appl. Phys. Lett*. 73:151–153.

Cricenti, A., R. Generosi, C. Barchesi, M. Luce, M. Rinaldi, C. Coluzza, P. Perfetti, G. Margaritondo, D. T. Schaafsma, I. D. Aggarwal, J. M. Gilligan, and N. H. Tolk. 1998b. First experimental results with the free electron laser coupled to a scanning near-field optical microscope. *Physica Status Solidi A*. 170:241–247.

Cricenti, A., R. Generosi, C. Barchesi, M. Luce, and M. Rinaldi. 1998c. A multipurpose scanning near-field optical microscope: reflectivity and photocurrent on semiconductor and biological samples. *Rev. Sci. Instrum.* 69:3240–3244.

Cricenti, A., R. Generosi, M. Luce, P. Perfetti, G. Margaritondo, D. B. Talley, J. S. Sanghera, I. D. Aggarwal, and N. H. Tolk. 2002. Very high resolution near-field chemical imaging using an infrared free electron laser. *Phys. Chem. Chem. Phys*. 4:2738–2741.

de Beer, D., P. Stoodley, F. Roe, and Z. Lewandowski. 1994. Effects of biofilm structures on oxygen distribution and mass-transport. *Biotechnol. Bioeng*. 43:1131–1138.

Diem, M., S. Boydston-White, and L. Chiriboga. 1999. Infrared spectroscopy of living cells and tissues: shining light onto a novel subject. *Appl. Spectrosc*. 53:148A–161A.

Heinzelmann, H., and D. W. Pohl. 1994. Scanning near-field optical microscopy. *Appl. Phys. A*. 59:89–101.

Hong, M. K., A. G. Jeung, N. V. Dokholyan, T. I. Smith, H. A. Schwettman, P. Huie, and S. Erramili. 1998. Imaging single living cells with a scanning near-field infrared microscope based on a free electron laser. *Nucl. Instr. Meth. Phys. Res. B*. 144:246–255.

Knoll, B., and F. Keilmann. 1999. Near-field probing of vibrational absorption for chemical microscopy. *Nature*. 399:134–137.

Lasch, P., A. Pacifico, and M. Diem. 2002. Spatially resolved IR microspectroscopy of single cells. *Biopolymers*. 67:335–338.

Margaritondo, G., F. Gozzo, and C. Coluzza. 1993. Band bending at semiconductor interfaces and its effect on photoemission line shapes. *Phys. Rev. B*. 47:9907–9909.

Michaels, C. A., S. J. Stranick, L. J. Richter, and R. R. Cavanagh. 2000. Scanning near-field infrared microscopy and spectroscopy with a broad-band laser source. *J. Appl. Phys*. 88:4832–4839.

Palanker, D. V., G. M. H. Knippels, T. I. Smith, and H. A. Schwettman. 1998. Fast IR imaging with sub-wavelength resolution using a transient near-field probe. *Nucl. Instr. Meth. Phys. Res. B*. 144:240–245.

Piednoir, A., C. Licoppe, and F. Creuzet. 1996. Imaging and local infrared spectroscopy with a near field optical microscope. *Opt. Comm*. 129:414–422.

Pohl, D. W., and D. Courjon, editors. 1992. Near-field optics. *In* NATO ASI Series, Vol. 262. Kluwer Academic Press, Boston, MA.

Talley, D. B., L. B. Shaw, J. S. Sanghera, I. D. Aggarwal, A. Cricenti, R. Generosi, M. Luce, G. Margaritondo, J. M. Gilligan, and N. H. Tolk. 2000. Scanning near field infrared microscopy using chalcogenide fiber tips. *Mater. Lett*. 42:339–344.

Tuncel, E., J. L. Staehli, C. Coluzza, G. Margaritondo, J. T. McKinley, R. G. Albridge, A. V. Barnes, A. Ueda, X. Yang, and N. H. Tolk. Free-electron laser studies of direct and indirect two-photon absorption in germanium. 1993. *Phys. Rev. Lett*. 70:4146–4149.

van der Maas, J. H. 1972. Basic Infrared Spectroscopy, 2nd Ed. Heyden & Son Ltd., London, UK. pp.88–89.

Williamson, R. L., L. J. Brereton, M. Antognozzi, and M. J. Miles. 1998. Are artifacts in scanning near-field optical microscopy related to the misuse of shear force? *Ultramicroscopy*. 71:165–175.

Zenhausern, F., Y. Martin, and H. K. Wickramasinghe. 1995. Scanning interferometric apertureless microscopy: optical imaging at 10 Å resolution. *Science*. 269:1083–1085.